European Radiology (2020) 30:357–369
https://doi.org/10.1007/s00330-019-06352-z

MAGNETIC RESONANCE

MRI evidence of brain atrophy, white matter damage, and functional adaptive changes in patients with cervical spondylosis and prolonged spinal cord compression

Ángela Bernabéu-Sanz[1] · José Vicente Mollá-Torró[2] · Susana López-Celada[1] · Pedro Moreno López[2] · Eduardo Fernández-Jover[3,4]

Received: 27 February 2019 / Revised: 13 June 2019 / Accepted: 1 July 2019 / Published online: 26 July 2019

Abstract

Objectives To investigate the effect of cervical spondylosis (CS) in the brain with a combination of advanced neuroimaging techniques.

Methods Twenty-seven patients with CS and 24 age- and gender-matched healthy controls were studied. Disease severity was quantified using the Modified Japanese Orthopaedic Association Scoring System (mJOHA). Magnetic resonance (MR) imaging of the brain and spinal cord, functional MR imaging (fMRI) with a bilateral rest/finger-tapping paradigm, brain diffusion tensor imaging (DTI), voxel-based morphometry (VBM), and MR spectroscopy of the sensorimotor cortex were performed.

Results A total of 92.3% of patients had more than one herniated disc. In the MRI, 33.33% presented signs of myelopathy. The mJOHA score was 13.03 ± 2.83. Compared with controls, DTI results showed significant lower FA values in *Corpus callosum*, both corticospinal tracts and middle cerebellar peduncles ($p < 0.05$ corrected). Only in CS patients fMRI results showed activation in both *globus pallidi*, caudate nucleus, and left thalamus ($p < 0.001$). Subject-specific activation of the BOLD signal showed in CS patients lower activation in the sensorimotor cortex and increased activation in both cerebellum hemispheres ($p < 0.05$ corrected). VBM showed bilateral clusters of gray matter loss in the sensorimotor cortex and pulvinar nucleus ($p < 0.05$ corrected) of CS patients. NAA/Cr was reduced in the sensorimotor cortex of CS patients ($p < 0.05$). Linear discriminant and support vector machine analyses were able to classify > 97% of CS patients with parameters obtained from the fMRI, DTI, and MRS results.

Conclusion CS may lead to distal brain damage affecting the white and gray matter of the sensorimotor cortex causing brain atrophy and functional adaptive changes.

Key Points

- *This study suggests that patients with cervical spondylosis may present anatomical and functional adaptive changes in the brain.*
- *Cervical spondylosis may lead to white matter damage, gray matter volume loss, and functional adaptive changes in the sensorimotor cortex.*
- *The results reported in this work may be of value to better understand the effect of prolonged cervical spine compression in the brain.*

Keywords Spondylosis · Spine · Brain · Neural plasticity

Electronic supplementary material The online version of this article (https://doi.org/10.1007/s00330-019-06352-z) contains supplementary material, which is available to authorized users.

✉ Ángela Bernabéu-Sanz
angela.bernabeu@gmail.com

[1] Magnetic Resonance Department, Inscanner SL, C/San Pedro Poveda, 10, 03010 Alicante, Spain

[2] Department of Neurosurgery, Hospital General Universitario de Alicante, Alicante, Spain

[3] Instituto de Bioingeniería, Universidad Miguel Hernández, Elche, Spain

[4] Centro de Investigación Biomédica en Red (CIBER BBN), Madrid, Spain

Abbreviations

CC	*Corpus callosum*
CG	Cingulum
Cho	Choline
Cr	Creatine
CS	Cervical spondylosis
CSM	Cervical spondylosis myelopathy
CST	Corticospinal tract
DTI	Diffusion tensor imaging
EMG	Electromyography
FA	Fractional anisotropy
fMRI	Functional magnetic resonance imaging
Glx	Glutamate and glutamine
MCP	Middle cerebellar peduncle
MD	Mean diffusivity
mIno	Myoinositol
mJOHA	Modified Japanese Orthopaedic Association Scoring System.
MR	Magnetic resonance
NAA	*N*-Acetyl aspartate
RD	Radial diffusivity
SMA	Supplementary motor area
TBSS	Tract-based spatial statistics
VBM	Voxel-based morphometry

Introduction

Cervical spondylosis (CS) is a chronic degenerative disease present in the majority of people after the fifth decade of life [1]. Frequently found in asymptomatic adults, it may progress to spinal cord compression and cervical spondylotic myelopathy (CSM) [2]. The evolution from CS to CSM is highly variable and difficult to predict, with patients experiencing a rather benign form of the disease while others experiencing substantial deterioration over time [3]. Generally, the treatment for mild and moderate disease is conservative, with surgical intervention advised for patients with severe intractable pain, progressive disease, or associated neurological deficits [4]. Yet, in some patients with mild or moderate disease, the absence of pain and the imprecision of the clinical manifestations could mask the development of a severe CSM [5].

Despite the potential irreversible neurological deficits of CS, its pathophysiology is still poorly understood. The majority of the studies have been focused on the spinal cord overlooking its connection with the cortex [6–10], with few studies analyzing the effects of CSM in the brain, suggesting that CSM can lead to neuronal damage distal to the spinal lesion [11–13] and functional reorganization of the sensorimotor cortex [14] that could be relevant for postsurgical recovery [15].

Taking into account the high prevalence of CS in the population and its putative associated secondary brain injury, the purpose of this work was to elucidate the effects of CS in the brain through a combination of advanced MR imaging techniques. Our hypothesis is that advanced MR techniques will detect the specific secondary brain damage caused by CS and that the observed results will help to classify the patients in the clinical setting, aiding clinicians in a better management of the disease.

Materials and methods

Participants

Twenty-seven right-handed subjects (14 females, 13 males, 55.92 ± 11.98 years) with CS attending the Department of Neurosurgery at the "Hospital General Universitario de Alicante" (Alicante, Spain) and 24 healthy controls (HC) (23 right-handed, 1 left-handed; 12 females, 12 males; 55.79 ± 12.12 years) eligible to undergo MR techniques were recruited.

Exclusion criteria were previous cervical spine surgery; neurologic, psychiatric, or systemic illness; previous head injury with loss of consciousness; presence of a non-MR imaging–compatible implant; musculoskeletal, degenerative joint disease or any other medical cause for weakness or pain affecting the hand and gait; history of alcohol or substance abuse; and severe claustrophobia.

The protocol was approved by the institutional review board. All participants were informed about the nature of the study and gave their written informed consent prior to entering the study.

Clinical examination

All patients underwent a clinical examination before (1.3 ± 0.5 months) and after the MR study (8 ± 1.5 months). Patients were classified according to clinical history, physical examination, and symptoms. Symptoms were classified as cervicalgia, cervicobrachialgia, and other (hand clumsiness, gait imbalance, tetraparesis, etc.). Disease evolution was classified as acute when the first symptoms appeared in ≤ 6 months, subacute when symptoms started between 6 months and 2 years, and chronic when the symptoms were present for ≥ 2 years. Disease evolution included hyperreflexia, extremities spasticity, intrinsic muscle atrophy, Hoffmann reflexes, hand stiffness, and gait dysfunction (stiff or spastic). Additionally, manual clumsiness, urination urgency, and patients' symptoms were included. In all cases, the Modified Japanese Orthopaedic Association Scoring System (mJOHA) scale was evaluated [2].

MR imaging

Scans were acquired in a Philips Achieva 3 T serie-X (Philips Medical) with a SENSE-Neurovascular coil. The protocol included brain axial T2-FLAIR, T2W-FFE, DWI/SE, and sagittal 3D-T1-wi and axial cervical spinal cord T2W_FFE, sagittal T2W_TSE, and STIR images (Supplementary Material).

MR images were analyzed by an expert radiologist (S. L-C) who assured the suitability of all participants and ruled out any brain pathology (i.e., tumors, previous stroke, gross anatomical malformations). Cervical spinal stenosis was measured in the sagittal plane at the middle of the intervertebral disc (from C1-C2 to C7-D1). The intramedullary spinal cord changes in signal intensity related to myelopathy were graded based on T2-wi in three levels as described previously [16].

Diffusion tensor imaging

Diffusion tensor imaging (DTI) was performed in an axial plane using a single-shot EPI sequence with diffusion encoding in 32 directions (Suppl. Material). We used FSL vs 5.0 (https://fsl.fmrib.ox.ac.uk) for preprocessing (head motion and eddy current distortion correction, diffusion tensor fitting) with FMRIB's Diffusion Toolbox (FDT v3.0) and tract-based spatial statistics (TBSS; http://www.fmrib.ox.ac.uk/fsl/tbss/). For TBSS analysis, skeletonized FA maps were analyzed with a voxel-wise cross-subject nonparametric analysis using the randomized tool (5000 permutations, 0.25 threshold) including age and sex as nuisance covariates. FWE-corrected maps for multiple comparisons were obtained with p values < 0.05 at cluster level and the white matter regions with statistically significant lower FA values were identified with the probabilistic digital atlas in FSL [17] and selected for tractography.

For tractography, preprocessing (eddy current distortions, head motion correction), and fiber tract generation, we used ExploreDTI [18] with a non-linear least square approach [19]. DTI scalar maps (FA, mean diffusivity (MD), radial diffusivity (RD)) were calculated and the whole brain tractography was performed with a FA > 0.2 threshold. Streamlines were propagated using a Euler integration [20] and a tractography algorithm step size of 1 mm. We performed virtual dissections of *corpus callosum* (CC), both corticospinal tracts (CSTs), cingulum (CG), and middle cerebellar peduncles (MCP) [21] using one or two regions of interest approach.

Functional MR imaging

A bilateral rest/tapping block paradigm was used [22]. Instructions were presented visually with a compatible system (VisuaStim Digital Glasses). Images were acquired throughout a blood oxygenation level-dependent sensitive T2-wi multi-slice gradient-echo EPI sequence (Suppl. Material). Analyses were performed with SPM8 (https://www.fil.ion.ucl.ac.uk/spm/software/spm8/); preprocessing steps included motion correction, registration with the 3D-T1-wi, spatial normalization to MNI space, and spatial smoothing (Gaussian kernel 8 mm). The preprocessed images were analyzed on an individual level with a general linear model, and contrast maps from individual subjects were entered into a group-level random-effects analysis. A 2-sample t test was carried out for group comparisons, and differences between groups were considered statistically significant at a voxel level of uncorrected $p < 0.001$ and a cluster ≥ 10 voxels. The coordinates reported by SPM were transformed to the stereotaxic coordinate for anatomical localization. To further investigate the local differences in the activation pattern, we used the MARSBAR tool in SPM [23]. Subject-specific first-level parameter estimation (beta-maps) was entered into the MarsBaR toolkit and the model beta coefficients and T-statistics were calculated for each ROI and extracted for group analysis.

MR spectroscopy

A short-echo-time PRESS sequence was used (Suppl. Material). For an optimal voxel placement, the functional MR imaging (fMRI) images were analyzed in the scanner console with the tool provided by the manufacturer. This analysis allowed us to locate the activated areas in each participant and therefore the specific region in the sensorimotor cortex for MR spectroscopy. All voxels presented the same dimensions $2 \times 2 \times 2$ cm and were placed over the frontal midline centered on the supplementary motor area (SMA) and at the activated areas in both central sulci (Fig. 1, Suppl. Material). Spectrum analysis was performed off-line with MRUI [24] as described previously [25–27].

Voxel-based morphometry

We used SPM8. Preprocessing steps included origin setting at the anterior commissure, gray and white matter segmentation, normalization with DARTEL toolbox, and smoothing with an 8-mm full width at half maximum. Total gray matter, white matter, and cerebrospinal fluid volumes were calculated with BRAIM software [28]. To identify brain regions with significant group differences in gray matter volume, a two-sample t test between groups was performed. Age, gender, and total intracranial volume were included as nuisance covariates. Statistical maps were corrected for multiple comparisons by FDR ($p < 0.05$) on the voxel level.

Statistical analysis

We used SPSS software (SPSS 20.0). Age and sex differences between groups were tested by t test and chi-square test, respectively. Quantitative variables are expressed as mean ±

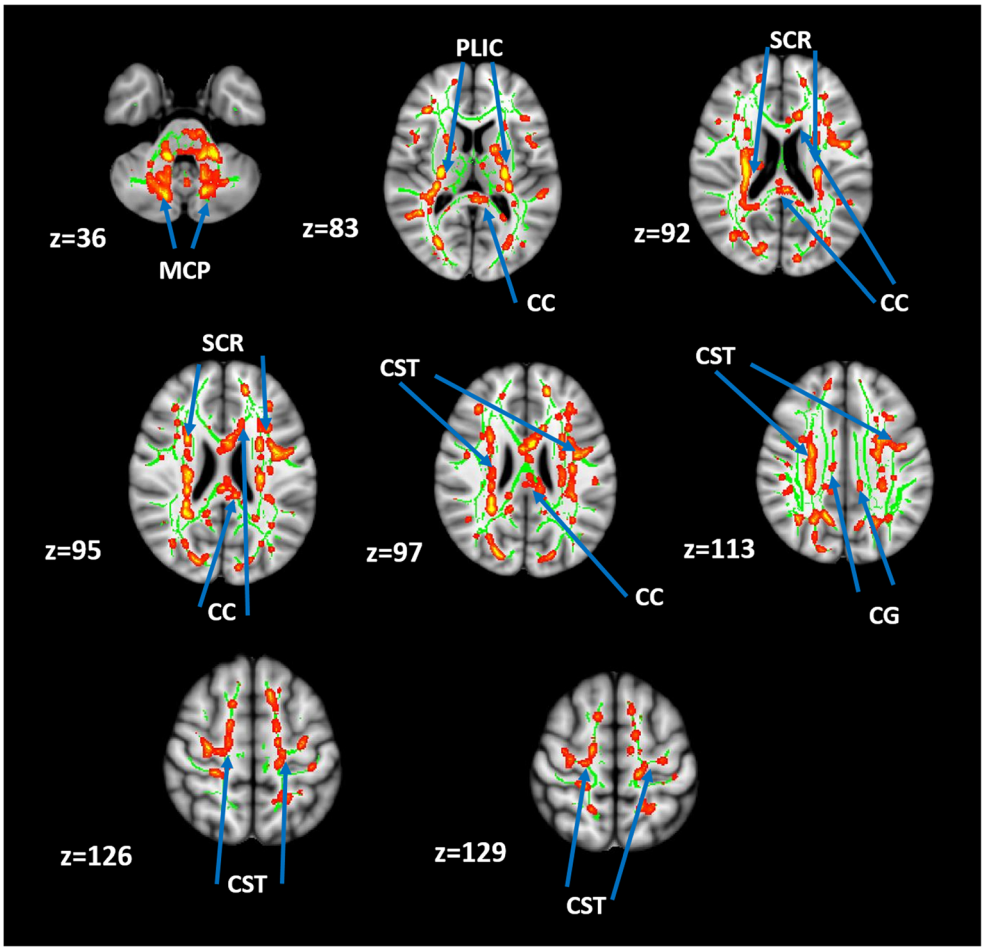

Fig. 1 TBSS analysis results of differences in fractional anisotropy between CS patients and controls in the *z* plane. Red-yellow scale regions indicate the areas with reduced fractional anisotropy values in the CS group. The thresholded stat image has been thickened for better perception. CC, *corpus callosum*; CG, cingulum; PLIC, posterior limb of the internal capsule; SCR, superior *corona radiata*; CST, corticospinal tract; MCP, middle cerebellar peduncle

standard and qualitative as percentages. The Kolmogorov–Smirnoff test was used to determining the normal distribution of variables. Changes in variables were tested with the paired Student *t* test. The Pearson rank correlation test (variables with normal distribution) and the Spearman rank correlation test (variables not adjusted to a normal distribution) were used. In all cases, a $p < 0.05$ was considered statistically significant.

To investigate the relative importance of the different MR imaging techniques, we performed a linear discriminant analysis (LDA). This approach allowed to effectively separate one dependent variable (CS group) as a linear combination of different measures from fMRI, DTI, and MR spectroscopy. A step-wise analysis was performed using standard criteria for entering and/or removing individual predictor variables. The multi-class classifiers were all based on the efficient nearest-neighbor classification scheme and evaluated by leave-one-subject-out cross-validation. It implies allocating each subject to its closest group without using that individual (but the remaining n-1 cases) to calculate the discriminant functions and then classify the left out case. Additionally, since LDA could provide overfitting of the data, we also used a support vector machine (SVM) classifier that has regularization methods to deal with complex data and avoid overfitting. Normalization was performed using a robust scale transform that removes the median and scales the data according to the quantile range (IQR) to avoid the possible effect of outliers, and the leave-one-out cross-validation method was used. For all these analyses, we used the Scikit-Learn free machine learning library for Python [29].

Results

Clinical characteristics

CS and HC groups were not significantly different in age and sex (p, 0.82; p, 0.72, respectively). CS etiology was compressive in all cases (26 patients related to disc degeneration, 1 patient from traumatic origin). In total, 88.8% of the patients were chronic (Table 1). The main symptom was unilateral cervicobrachialgia (8 affecting the left upper limb, 6 affecting the right upper limb). Eight patients presented clear signs of myelopathy in the physical examination, and 11 presented pathological EMG results suggesting nerve radiculopathy. The initial mJOHA score was 13.03 ± 2.83 (range 7–17).

Table 1 Clinical features and MR imaging results of the CS group

$n = 27$	Description		Number of cases
Symptoms	Cervicalgia		2 (7.4%)
	Cervicobrachialgia	Unilateral	14 (51.85%)
		Bilateral	5 (18.58%)
	Others	Tetraparesia	2 (7.4%)
		Manual clumsiness and gait imbalance	3 (11.1%)
		Hypoesthesia	1 (3.7%)
Evolution	Acute		1 (3.7%)
	Subacute		2 (7.4%)
	Chronic		24 (88.8%)
Myelopathy in MRI	Grade 1	1 level, 6 (22.22%)	14 (51.85%)
		> 1 level, 8 (29.63%)	
	Grade 2	1 level, 5 (18.51%)	9 (33.33%)
		> 1 level, 4 (14.81%)	
Lordosis loss	Mild, 6 (22.22%)		Normal, 3 (11.11%)
	Marked, 10 (37.03%)		Altered, 24 (88.88%)
	Marked with inversion, 8 (29.63%)		
Herniated discs (*n*)/patient	Posteromedial, 16 (18.82%)		2.93 ± 1.18 (range 1–6)
	Right para-median, 3 (3.53%)		
	Left para-median: 3 (3.53%)		
	Bilateral para-median, 1 (1.17%)		
	Right foraminal, 3 (3.53%)		
	Diffuse, 55 (64.70%)		
	Migrated disc, 4 (4.7%)		
Osteoarthritis	Affecting 1 level, 4 (16%)		25 (92.59%)
	Affecting > 1 level, 21 (84%)		

Fifteen patients (55%) underwent surgery because of clinical worsening, with an averaged time after the MR of 5.35 ± 3.67 months. The surgical techniques included anterior (96%) and posterior approaches (4%). No surgical complications were observed. Six months after surgery, no significant differences were observed in the mJOHA scores (preoperative 14.12 ± 2.3, postoperative 14.75 ± 1.94; *p*, 0.1). However, 73.33% of the patients related a substantial decrease in the level of pain.

Neuroimaging analyses

Cervical MR imaging

All patients but two had more than one herniated disc (Table 1). A total of 33.33% of the patients presented myelopathy grade 2 in the MR. The most common type of herniated disc was diffuse. All patients but two presented osteoarthritis.

DTI

TBSS results showed statistically significant lower FA values (corrected for multiple comparisons) in CS patients in the CC, both posterior limbs of the internal capsule, *corona radiata*, CST, CG, and MCP (Fig. 1).

Manual dissection of the affected white matter tracts showed reduced FA values in all the fibers dissected, with a statistically significant reduction of the streamlines in the CC, both CSTs, and left CG (Table 2). MD values were also increased in the CC and both CSTs.

3D visualization of the CST dissections suggested that the observed streamline reduction was located mainly at the anterior-distal segment. This result was observed in 14 patients (51.85%, 7 cases bilaterally, 7 cases unilaterally (2 affecting the left and 5 affecting the right hemisphere, Fig. 2)). 3D visualization of the CC showed in 20 patients (74%) a significant reduction in the streamlines (Fig. 2). The most common affected area was the posterior parietal projection fibers ($n = 13$, 5 bilateral, 8 affecting the right hemisphere). Seven patients presented wider damage affecting both hemispheres at different locations within the CC from the genu to splenium. In all cases, commissural fibers were preserved.

Finally, in the CS group, we observed that patients with right cervicobrachialgia ($n = 6$) when compared

Table 2 Tract-specific result comparisons after manual dissection of the white matter tracts between CS and HC groups. *p* values are an unpaired two-tailed test between groups; only statistically significant results are shown

	Patients	Controls	*p* values
CC FA values	0.48 ± 0.03	0.54 ± 0.02	0.000
CC MD values	0.91 ± 0.12	0.84 ± 0.09	0.03
CC STR	12183.3 ± 4939	14968.4 ± 3810.4	0.04
Left CST FA values	0.46 ± 0.03	0.49 ± 0.02	0.01
Left CST MD values	0.82 ± 0.05	0.77 ± 0.07	0.007
Left CST STR	2641.2 ± 1531.2	4051.4 ± 1179.16	0.002
Right CST FA values	0.46 ± 0.03	0.5 ± 0.03	0.001
Right CST MD values	0.82 ± 0.08	0.74 ± 0.06	0.001
Right CST STR	2840.1 ± 1564.2	4295.85 ± 1235.7	0.001
Left GG FA values	0.41 ± 0.03	0.46 ± 0.02	0.000
Left GG STR	1091.6 ± 454	1499.35 ± 584.24	0.012
Right CG FA values	0.43 ± 0.04	0.48 ± 0.03	0.000
Left MCP FA values	0.44 ± 0.03	0.5 ± 0.02	0.000
Right MCP FA values	0.45 ± 0.03	0.51 ± 0.02	0.000

with left cervicobrachialgia ($n = 8$) presented significant higher MD values in the left corticospinal tract (p, 0.04). No other significant differences were observed between the patients' symptoms in the CS group.

MR spectroscopy

A statistically significant decrease in the NAA/Cr and Cho/Cr ratios in all the motor areas studied in CS patients was observed (Table 3). Moreover, both primary motor areas presented a significant reduction in the mIno/Cr ratio when compared with controls. No other significant differences were observed.

fMRI

We found bilateral activation of the pre- and postcentral gyrus along the central sulcus in all subjects, reflecting activation of the primary sensorimotor cortex [30]. Compared with controls, CS patients showed a higher number of activated brain areas including *globus pallidus*, left thalamus, and caudate nucleus, as well as increased activation in both cerebellum hemispheres (Fig. 3a, Table 4). Subject-specific activation of the BOLD signal determined by the beta-values extracted from the MarsBaR analyses (Fig. 3b) showed that the CS group presented statistically significant lower activation in SMA and both sensorimotor cortices, whereas an increased activation in both cerebellum hemispheres.

Moreover, in the CS group, it was observed lower beta-values in the left motor cortex (p, 0.039) in patients with right cervicobrachialgia when compared with patients with left cervicobrachialgia. No other significant differences were observed.

VBM

We observed significant clusters of gray matter loss in CS patients affecting both primary sensorimotor cortices and both thalami, specifically at the pulvinar nucleus (Table 5, Fig. 4). Characteristically, the activated motor areas in the fMRI analysis in the CS group were located in the periphery of the clusters of gray matter loss (Fig. 5). No other significant differences were observed.

Correlations

Patients' mJOHA correlated with the streamlines at the right CST (r, 0.6; p, 0.01) and CC (r, 0.5; p, 0.02), right CG FA, and streamlines values (r, 0.48; p, 0.16 and r, 0.5; p, 0.011, respectively) and the NAA/Cr ratio at the right motor cortex (r, − 0.53; p, 0.005).

A negative correlation was observed between the myelopathy grade in the cervical MR imaging and the NAA/Cr ratio in SMA (r, − 0.71; p, 0.002) and left motor cortex (r, − 0.56; p, 0.03).

Patients' evolution after surgery negatively correlated with the streamlines at the right (r, − 0.63; p, 0.02) and left (r, − 0.62; p, 0.02) CSTs.

Finally, a negative correlation was observed between the streamlines at the right CST and the evolution time of the disease (r, − 0.45; p, 0.03). Moreover, a positive correlation was observed between the observed reduction of streamlines in the anterior-distal segment in the 3D visualization of the

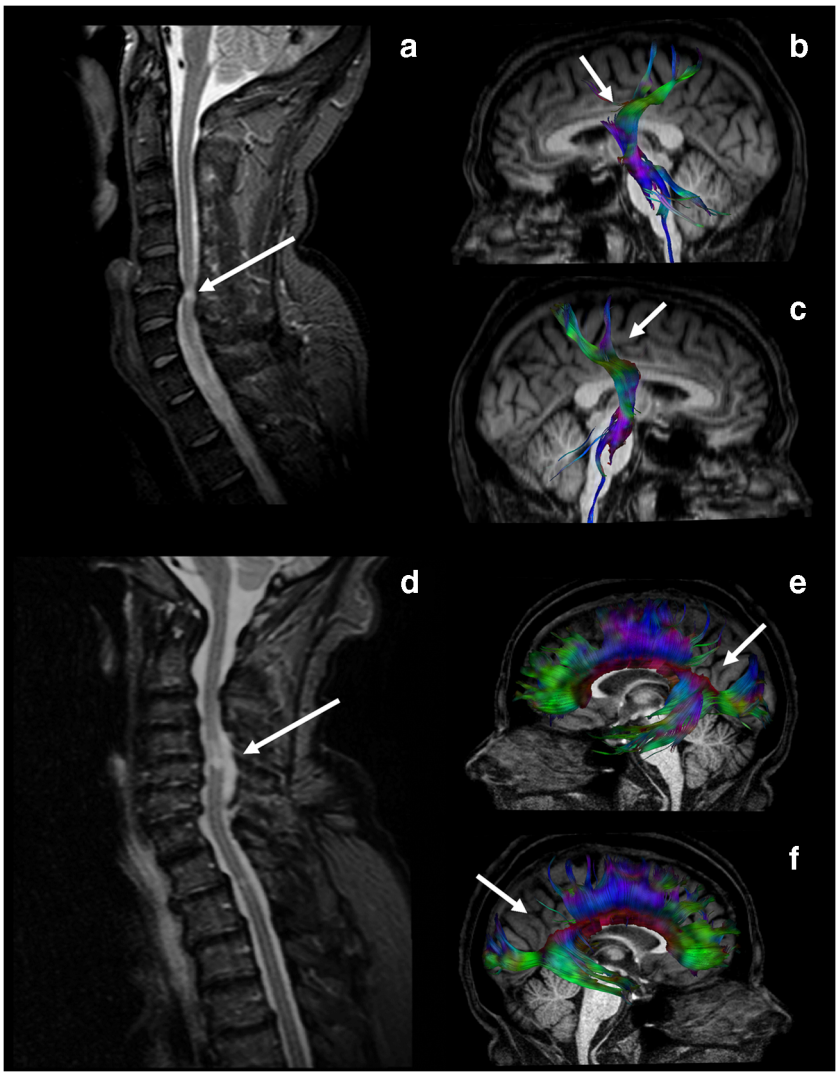

Fig. 2 **a** Sagittal STIR of a 47-year-old male patient with chronic right cervicobrachialgia and a para-median herniated disc (see arrow). The patient presented myelopathy at C5-C6 level and significant cervical lordosis loss. **b**, **c** Tractography results suggested significant bilateral and symmetrical axonal damage affecting both corticospinal tracts at the distal-anterior regions (see arrows) at both *corona radiata* levels. **d** Sagittal STIR of a 48-year-old female patient with chronic left cervicobrachialgia. The patient presented a diffuse herniated disc at C5-C6 and a bilateral para-median herniated disc at C6-C7 and significant cervical lordosis loss. **e**, **f** Fiber tracking tractography results suggested the presence of myelin damage at the *corpus callosum*, specifically a bilateral myelin loss at the posterior parietal projection fibers. Commissural fibers were preserved

dissected right CST and the surgery performance (r, 0.67; p, 0.001).

Discriminant analysis

LDA results showed that the main measures used for the classification task were DTI (FA values at left CST, CC, and both MCPs) together with the β-values at the left motor cortex and MR spectroscopy (NAA/Cr at SMA and left motor cortex). In fact, using just these measures, it was possible to correctly classify 97.3% of individuals as HC or CS subjects (Fig. 6), which emphasizes the relevance and discriminative role of this advanced neuroimaging techniques. These results were also corroborated with the SVM analysis, where it was possible to correctly classify the 98% of individuals as HC or CS subjects with the same MRI parameters.

Discussion

The present study explores the distal effects of CS in the brain. Our results suggest that prolonged cervical spine compression may lead to distal damage to the white matter tracts and gray matter, causing brain atrophy of the sensorimotor cortex and thalami, and functional reorganization.

We found in CS patients white matter damage in both CSTs, supporting previous studies that proposed the demyelination of the CST fibers as the predominant pathological mechanism of CSM that causes a progressive loss of axonal conduction [15]. In animal models, chronic CS causes inflammation and apoptosis of the motor neurons in the anterior horn causing demyelination of the CSTs [31]. Our results uphold these findings proposing that the integrity of the CSTs may present a key role in the development of CSM, as its integrity in our patient group is associated with the mJOHA scores, the

Table 3 MR spectroscopy results. Values are given as mean ± SD. *p* values are unpaired two-tailed test comparisons between CS and HC groups

	Patients	Controls	*p*
NAA/Cr SMA	1.33 ± 0.20	1.69 ± 0.21	0.000
NAA/Cr left motor area	1.42 ± 0.24	1.9 ± 0.29	0.000
NAA/Cr right motor area	1.48 ± 0.20	1.74 ± 0.19	0.000
Cho/Cr SMA	0.73 ± 0.09	0.83 ± 0.18	0.028
Cho/Cr left motor area	0.66 ± 0.12	0.82 ± 0.22	0.004
Cho/Cr right motor area	0.64 ± 0.10	0.75 ± 0.11	0.001
Glx/Cr SMA	1.99 ± 0.97	2.08 ± 0.39	0.7
Glx/Cr left motor area	2.21 ± 0.87	1.88 ± 0.59	0.13
Glx/Cr right motor area	1.94 ± 0.97	1.94 ± 0.52	0.99
mIno/Cr SMA	0.50 ± 0.08	0.58 ± 0.19	0.077
mIno/Cr left motor area	0.48 ± 0.14	0.58 ± 0.21	0.045
mIno/Cr right motor area	0.44 ± 0.16	0.53 ± 0.13	0.049

evolution time of the disease, and the postoperative clinical evolution. A previous study by Lee et al reported with DTI better surgical outcomes in patients with intact long tracts at the spinal cord [32]. In this context, the reduced number of streamlines observed in our patients in the CSTs may lead to some critical threshold to impairment explaining, at least partially, why it was not observed a significant improvement on the postoperative mJOHA scores [33].

We also found in CS a reduction in the CC streamlines, primarily in the parietal and posterior parietal projection fibers, which are mainly related to motor and touch stimulation [34]. The MR spectroscopy analysis supports these findings suggesting neuronal and/or axonal damage in both primary sensorimotor cortices and SMA. Similar findings were reported by Kowalczyk et al in CSM [13], but the authors only studied the primary sensorimotor cortex related to the limb with the greater functional deficit. Our results go further proposing that there could be damage at both primary sensorimotor cortex and SMA, independently of the affected limb. Interestingly, we found a negative correlation between the NAA/Cr levels at SMA and the myelopathy degree in the MR imaging study, suggesting that CS may lead to neuronal and/or axonal damage in the sensorimotor cortex. Besides, the voxel-based morphometry (VBM) analysis showed significant clusters of gray matter loss in CS patients in both primary sensorimotor cortex and thalami suggesting that CS may also induce brain atrophy. These results are in line with previous studies in CSM that reported a reduction in the thalamo-sensorimotor connectivity, proposing it as an underlying biomarker for disease severity and

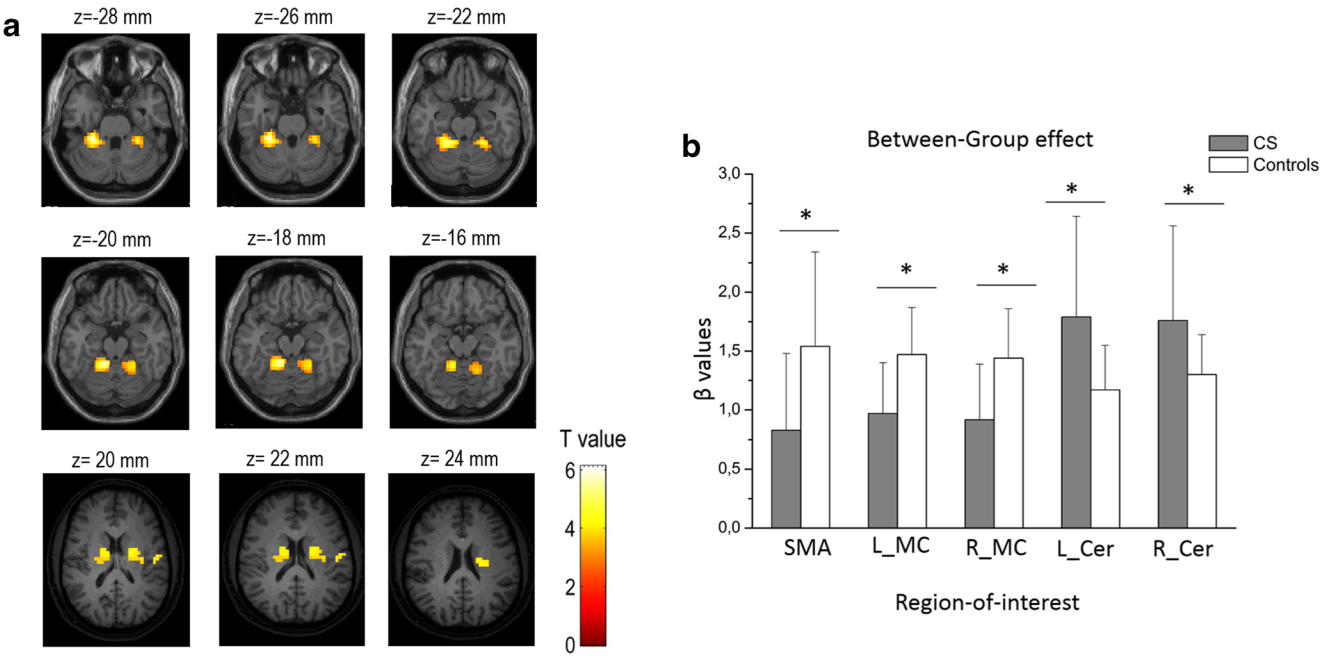

Fig. 3 **a** fMRI activation maps showing group differences after a second-level analysis across both groups superimposed in the *z* plane through the T1 MNI average brain. The results correspond to Table 3 results. **b** Extracted beta-values (contrast parameter estimates) from MarsBaR in each region of interest for CS patients and controls. Error bars represent standard error and the asterisk denotes a significant difference ($p < 0.05$) between groups. SMA, supplementary motor area; L_MC, left sensorimotor cortex; R_MC, right sensorimotor cortex; L_Cer, left cerebellum hemisphere; R_Cer, right cerebellum hemisphere

Table 4 Brain activation pattern differences after group comparison

Brain area	Hemisphere	BA	*x*	*y*	*z*	*z* score	Cluster	*p* value[a]
Control < patients								
Cerebellum culmen	L		− 28	− 37	− 26	5.17	112	< 0.001
			− 13	− 44	− 18	4.82		< 0.001
			− 21	− 44	− 22	4.64		< 0.001
Cerebellum tonsil	L		− 21	− 55	− 46	4.47	17	< 0.001
Cerebellum inferior semi-lunar lobule	L		− 13	− 62	− 42	3.8		< 0.001
Cingulate gyrus	R	31	26	− 40	26	4.42	73	< 0.001
Caudate body	R		15	− 8	22	3.79	28	< 0.001
	R		15	− 15	26	3.58		< 0.001
Claustrum	R		26	− 15	22	3.27		< 0.001
Insula	R	13	44	− 11	18	3.68	12	< 0.001
Caudate body	L		− 21	− 8	22	3.54	24	< 0.001
Claustrum	L		− 28	− 19	18	3.24		< 0.001

[a] $p < 0.001$ uncorrected. The reverse contrast "controls > patients" yielded no significant results

progression [35–37]. According to our results, this connectivity reduction may be related to the observed gray matter loss.

During the bilateral finger-tapping task, we found in CS patients an increased activation in the cerebellum and basal ganglia. Similar findings have been described in patients with spinal cord injury [38, 39] inferring the possible existence of some basic reorganization of the neural activity within the supraspinal motor centers [39–41] that appear to be more significant for finger and hand movements [42]. The cerebellum processes the afferent inputs from the spinal cord, whereas the thalamus is a relay nucleus to the motor cortex with internal loops from the basal ganglia and the cerebellum. Hence, if CS originates a reduction in the afferent input from the spinal cord, it may cause stronger activation or disinhibition of the neuronal centers involved as a compensatory mechanism. Interestingly, the activated brain areas in the CS group appeared in the vicinity of the clusters with gray matter loss,

Table 5 Clusters of gray matter loss in the patient group. $p < 0.05$ corrected. The reverse contrast "controls < patients" yielded no significant results

Brain area	Hemisphere	BA	*x*	*y*	*z*	*T*	Cluster	*p* value
Control > patients								
Thalamus, pulvinar	R		14	− 26	10	11.91	14970	< 0.001
Thalamus, pulvinar	R		2	− 16	6	8.99		< 0.001
Thalamus, pulvinar	L		− 12	− 26	10	8.77		< 0.001
Precentral gyrus	R	BA4	50	− 12	44	9.94	46220	< 0.001
Postcentral gyrus	L	BA3	− 48	− 16	44	9.76		< 0.001
Frontal lobe, paracentral lobule	L	BA6	0	− 30	70	9.7		< 0.001
Temporal lobe, fusiform gyrus	R	BA37	56	− 50	− 20	9.34	106	< 0.001
Temporal lobe, fusiform gyrus	R	BA20	46	− 22	− 26	7.51	134	< 0.001
Insula	R	BA13	40	− 18	8	6.75	47	< 0.001
Cerebellum, posterior lobe, tuber	L		− 16	− 90	− 30	6.7	28	< 0.001
Frontal lobe, precentral gyrus	L	BA44	− 42	2	6	6.57	39	< 0.001
Frontal lobe, middle frontal gyrus	R	BA6	38	0	54	6.18	38	< 0.001
Frontal lobe, middle frontal gyrus	R	BA6	2	− 8	66	6.03	13	< 0.001

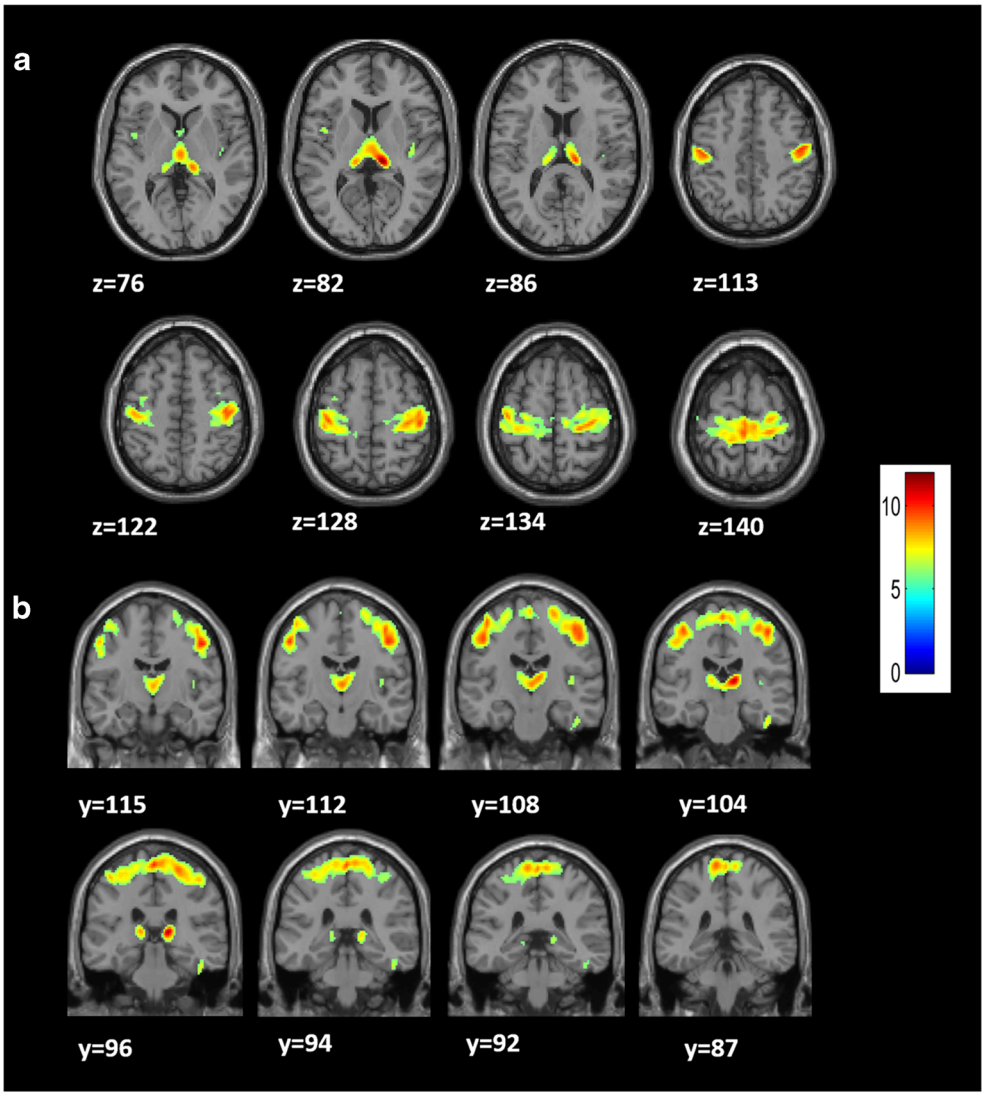

Fig. 4 Voxel-based morphometric analysis results in the *z* plane (**a**) and *y* plane (**b**) demonstrate clusters of significant cortical decreased volume in the CS group compared with controls ($p < 0.05$ corrected) affecting both primary sensorimotor areas and thalami

suggesting that the observed displacement and/or reorganization of the sensorimotor cortex reported by some authors [11, 43] might be mediated by adaptive changes to brain atrophy to preserve the "normal" hand function. Indeed, in a previous study by Henderson et al, the authors reported a direct association between the observed gray matter loss in the primary somatosensory cortex and its functional reorganization [44]. Moreover, this functional reorganization is closely associated with the severity of the cervical cord injury and the clinical presentation [14], helping to maintain a residual motor function limiting its deterioration and contributing to its restoration if the disease progression is halted [15].

Finally, using LDA and SVM analyses, we showed that CS patients could be correctly classified in > 97% of the cases with MR parameters related to the integrity of the sensorimotor cortex, CST, and CC, proposing that these brain areas may play a key role in the development of the disease.

Several limitations in the present study must be acknowledged. Firstly, the sample size did not allow us to detect subtle differences in the MR analysis with the patients' symptoms. Secondly, this study included short-term monitoring; a long-term monitoring study will be necessary to better establish the putative role of MR parameters as predictors of disease evolution and recovery. This will be addressed in future work. Finally, we did not measure the finger-tapping frequency performance in the task-related fMRI which may affect the hemodynamic response within the cortical regions and basal ganglia [45].

Overall, according to our results, prolonged CS could damage the CSTs, causing brain atrophy of the sensorimotor cortex and thalami and functional reorganization. These changes may be gradual allowing the brain to adapt through plasticity, causing the wide spectrum of clinical manifestations observed in CS. In this framework, the best timing for surgery to ensure neurological preservation has been discussed [12, 46] with a clear incentive to find a clinical method to predict neurological

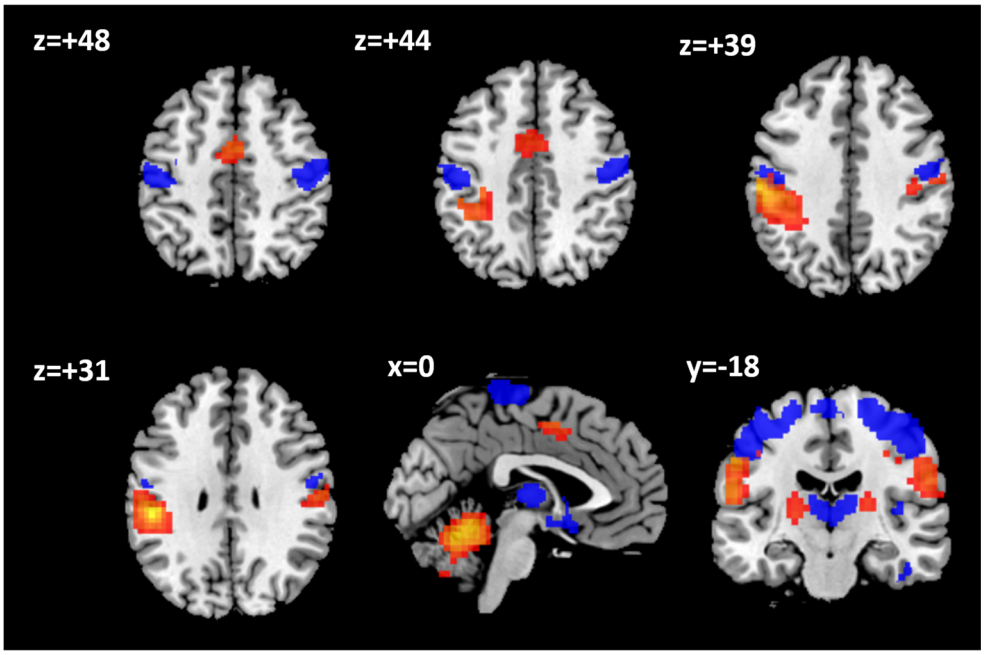

Fig. 5 Sagittal (*x* plane), axial (*z* plane), and coronal (*y* plane) images through the MNI average brain showing the CS group activation fMRI maps (yellow-red scale) and the VBM results (blue) superimposed ($p < 0.05$ corrected). The activated areas during the bilateral finger-tapping task appeared in the vicinity of the areas with gray matter loss observed in the VBM analysis

recovery. In animal models, it has been shown that surgical decompression in CS is able to partially restore function [47], which fits well with our results where we did not observe any significant recovery in the patients' symptoms at short-time monitoring, probably because of the chronicity of CS in our group. From this perspective, more work with longitudinal studies to clarify the precise temporal limits to avoid irreversible neurological injury is needed.

CSM is a common manifestation of CS; its prevalence is rising with the increase in life expectancy. Though the management of severe CSM is well-defined, there is no such consensus for its subtle forms. There is a lack of certainty concerning its course, with individuals experiencing a progressive decline while others having long periods of dormancy. While MRI plays an integral role in CSM diagnosis, it is likely to demonstrate a stable radiological appearance despite the progression of spinal cord injury and subsequent neurological symptomatology. This is mirrored in the poor correlation of conventional MRI data with neurological and functional impairment and its failure to provide reliable prognostic information [48]. According to our results, tract-specific degeneration of the CSTs secondary to CS can be detected with DTI. Importantly, these remote tract-specific changes are related to the clinical presentation and patients' evolution and may be applied as surrogate markers to assess secondary brain injury and monitor treatment effects with clinical outcome measures. Since CST preservation is crucial for successful brain rehabilitation and recovery [33], we propose DTI as a useful tool for prognosis related to interventions aimed at reducing the functional consequences of CSM.

a

	Controls	CS patients
FA values in Left CST	0.8	0.55
FA values in CC	1294.42	1165.15
FA values in Left MCP	589.27	502.95
FA values in Right MCP	-0.06	-0.05
NAA/Cr in SMA	165.47	131.91
NAA/Cr in left motor cortex	58.89	43.23
β-values in left motor cortex	16.31	9.85
Constant	-680.83	-494.7

b

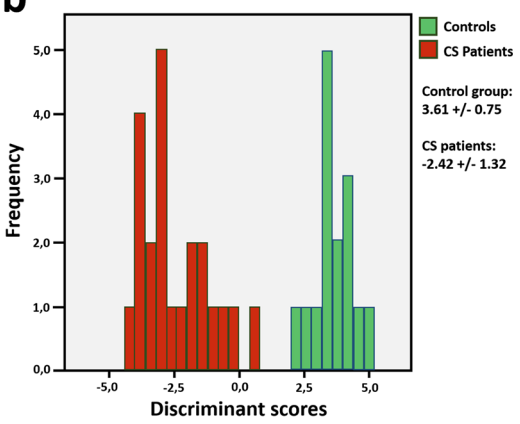

Fig. 6 **a** Summary of the linear discriminant analysis (LDA) model and classification results. Parameters and coefficients in the discriminant function (classification accuracy using these parameters and the leave-one-out cross-validation approach, 97.3%). **b** Discriminant score distribution and predicted classification results of all the cases using this discriminant function

In conclusion, although more studies are needed, this preliminary study exhibits the potential of using advanced neuroimaging techniques as a physiological assessment to examine patients with CS. Our results suggest that advanced neuroimaging techniques could be used as biomarkers to predict symptom development, helping to evaluate specific effects and/or rehabilitation strategies in CS, and could help in the controversy surrounding the management of asymptomatic patients.

Acknowledgments The authors would like to thank the following people: our subjects for their time and help. Our MR technologists Mr. David González García, Miss. Patricia Lucena Ibáñez, Ms. Evelyn Teruel Sanchez, and Ms. Maria Vicenta Picazo Panadero for their outstanding technical support during the acquisition of the studies. Mr. Mikel Val for his invaluable help and advice in the SVM analysis. We would also like to show our gratitude to the anonymous reviewers who provided insight and expertise that greatly improved the manuscript.

Funding This work was supported in part by Grant No. RTI2018-098969-B-100 from the Spanish Government and by the Bidons Egara Research Chair.

Compliance with ethical standards

Guarantor The scientific guarantor of this publication is Dr. Ángela Bernabeu-Sanz.

Conflict of interest The authors of this manuscript declare no relationships with any companies, whose products or services may be related to the subject matter of the article.

Statistics and biometry No complex statistical methods were necessary for this paper.

Informed consent Written informed consent was obtained from all subjects (patients) in this study.

Ethical approval Institutional Review Board approval was obtained.

Methodology
- prospective
- case-control study
- performed at one institution

References

1. Boden SD, McCowin PR, Davis DO, Dina TS, Mark AS, Wiesel S (1990) Abnormal magnetic-resonance scans of the cervical spine in asymptomatic subjects. A prospective investigation. J Bone Joint Surg Am 72:1178–1184
2. Bakhsheshian J, Mehta VA, Liu JC (2017) Current diagnosis and management of cervical spondylotic myelopathy. Global Spine J 7: 572–586. https://doi.org/10.1177/2192568217699208
3. Tracy JA, Bartleson JD (2010) Cervical spondylotic myelopathy. Neurologist 16:176–187
4. Lebl DR, Bono CM (2015) Update on the diagnosis and management of cervical spondylotic myelopathy. J Am Acad Orthop Surg 23:648–660
5. Clarke E, Robinson PK (1956) Cervical myelopathy: a complication of cervical spondylosis. Brain 79:483–510
6. Morishita Y, Naito M, Hymanson H, Miyazaki M, Wu G, Wang JC (2009) The relationship between the cervical spinal canal diameter and the pathological changes in the cervical spine. Eur Spine J 18: 877–883
7. Wada E, Yonenobu K, Suzuki S, Kanazawa A, Ochi T (1999) Can intramedullary signal change on magnetic resonance imaging predict surgical outcome in cervical spondylotic myelopathy? Spine (Phila PA 1976) 24:455–461 discussion 462
8. Stroman PW, Nance PW, Ryner LN (1999) BOLD MRI of the human cervical spinal cord at 3 tesla. Magn Reson Med 42:571–576
9. Okada E, Matsumoto M, Fujiwara H, Toyama Y (2011) Disc degeneration of cervical spine on MRI in patients with lumbar disc herniation: comparison study with asymptomatic volunteers. Eur Spine J 20:585–591
10. Xiangshui M, Xiangjun C, Xiaoming Z et al (2010) 3 T magnetic resonance diffusion tensor imaging and fiber tracking in cervical myelopathy. Clin Radiol 65:465–473
11. Duggal N, Rabin D, Bartha R et al (2010) Brain reorganization in patients with spinal cord compression evaluated using fMRI. Neurology 74:1048–1054
12. Holly LT (2009) Management of cervical spondylotic myelopathy with insights from metabolic imaging of the spinal cord and brain. Curr Opin Neurol 22:575–581
13. Kowalczyk I, Duggal N, Bartha R (2012) Proton magnetic resonance spectroscopy of the motor cortex in cervical myelopathy. Brain. https://doi.org/10.1093/brain/awr328
14. Zhou FQ, Tan YM, Wu L, Zhuang Y, He LC, Gong HH (2015) Intrinsic functional plasticity of the sensory-motor network in patients with cervical spondylotic myelopathy. Sci Rep 5:1–8. https://doi.org/10.1038/srep09975
15. Dong Y, Holly LT, Albistegui-Dubois R et al (2008) Compensatory cerebral adaptations before evolving changes after surgical decompression in cervical spondylotic myelopathy. J Neurosurg Spine 9: 538–551. https://doi.org/10.3171/SPI.2008.10.0831.Compensatory
16. Yukawa Y, Kato F, Yoshihara H, Yanase M, Ito K (2007) MR T2 image classification in cervical compression myelopathy. Spine (Phila PA 1976) 32:1675–1678. https://doi.org/10.1097/BRS.0b013e318074d62e
17. Oishi K, Zilles K, Amunts K et al (2008) Human brain white matter atlas: identification and assignment of common anatomical structures in superficial white matter. Neuroimage 43:447–457. https://doi.org/10.1016/j.neuroimage.2008.07.009
18. Leemans A, Jeurissen B, Sijbers J, Jones D (2009) ExploreDTI: a graphical toolbox for processing, analyzing, and visualizing diffusion MR data. Proc Intl Soc Mag Reson Med 17:3537
19. Jones DK, Basser PJ (2004) "Squashing peanuts and smashing pumpkins": how noise distorts diffusion-weighted MR data. Magn Reson Med 52:979–993. https://doi.org/10.1002/mrm.20283
20. Basser PJ, Pajevic S, Pierpaoli C, Duda J, Aldroubi A (2000) In vivo fiber tractography using DT-MRI data. Magn Reson Med 44:625–632. https://doi.org/10.1002/1522-2594(200010)44:4<625::AID-MRM17>3.0.CO;2-O
21. Wakana S, Jiang H, Nagae-Poetscher LM, van Zijl PC, Mori S (2004) Fiber tract-based atlas of human white matter anatomy. Radiology 230:77–87. https://doi.org/10.1148/radiol.2301021640
22. Papke K, Reimer P, Renger B et al (2000) Optimized activation of the primary sensorimotor cortex for clinical functional MR imaging. AJNR Am J Neuroradiol 21:395–401
23. Brett M, Anton J-L, Valabregue R, Poline J-B (2002) Region of interest analysis using an SPM toolbox [Internet]. Vol. 16, Presented at the 8th International Conference on Functional Mapping of the Human Brain. [cited 2019 Feb 18]. Available from:

https://matthew.dynevor.org/research/abstracts/marsbar/marsbar_abstract.pdf
24. Naressi A, Couturier C, Devos JM et al (2001) Java-based graphical user interface for the MRUI quantitation package. MAGMA 12: 141–152
25. Bernabeu A, Alfaro A, García M, Fernández E (2009) Proton magnetic resonance spectroscopy (1H-MRS) reveals the presence of elevated myo-inositol in the occipital cortex of blind subjects. Neuroimage 47:1172–1176. https://doi.org/10.1016/j.neuroimage.2009.04.080
26. Cano M, Martínez-Zalacaín I, Bernabéu-Sanz Á et al (2017) Brain volumetric and metabolic correlates of electroconvulsive therapy for treatment-resistant depression: a longitudinal neuroimaging study. Transl Psychiatry 7:e1023. https://doi.org/10.1038/tp.2016.267
27. Poveda MJ, Bernabeu Á, Concepción L et al (2010) Brain edema dynamics in patients with overt hepatic encephalopathy. A magnetic resonance imaging study. Neuroimage 52:481–487. https://doi.org/10.1016/j.neuroimage.2010.04.260
28. Morales S, Bernabeu-Sanz A, López-Mir F, González P, Luna L, Naranjo V (2017) BRAIM: a computer-aided diagnosis system for neurodegenerative diseases and brain lesion monitoring from volumetric analyses. Comput Methods Programs Biomed 145:167–179. https://doi.org/10.1016/j.cmpb.2017.04.006
29. Pedregosa F, Varoquaux G, Gramfort A et al (2011) Scikit-learn: machine learning in Python. J Mach Learn Res 12. Available from: http://scikit-learn.org
30. Schott GD (1993) Penfield's homunculus: a note on cerebral cartography. J Neurol Neurosurg Psychiatry 56:329–333
31. Ijima Y, Furuya T, Koda M et al (2017) Experimental rat model for cervical compressive myelopathy. Neuroreport 28:1239–1245. https://doi.org/10.1097/WNR.0000000000000907
32. Lee JW, Kim JH, Bin PJ et al (2011) Diffusion tensor imaging and fiber tractography in cervical compressive myelopathy: preliminary results. Skeletal Radiol 40:1543–1551. https://doi.org/10.1007/s00256-011-1161-z
33. Jang SH (2014) The corticospinal tract from the viewpoint of brain rehabilitation. J Rehabil Med 46:193–199. https://doi.org/10.2340/16501977-1782
34. Fabri M, Pierpaoli C, Barbaresi P, Polonara G (2014) Functional topography of the corpus callosum investigated by DTI and fMRI. World J Radiol 6:895–906. https://doi.org/10.4329/wjr.v6.i12.895
35. Zhou F, Gong H, Liu X, Wu L, Luk KD, Hu Y (2014) Increased low-frequency oscillation amplitude of sensorimotor cortex associated with the severity of structural impairment in cervical myelopathy. PLoS One. https://doi.org/10.1371/journal.pone.0104442
36. Zhou F, Wu L, Liu X, Gong H, Luk KD, Hu Y (2015) Characterizing thalamocortical disturbances in cervical spondylotic myelopathy : revealed by functional connectivity under two slow frequency bands. PLoS One https://doi.org/10.1371/journal.pone.0125913
37. Tan Y, Zhou F, Wu L et al (2015) Alteration of Regional homogeneity within the sensorimotor network after spinal cord decompression in cervical spondylotic myelopathy: a resting-state fMRI study. Biomed Res Int 647958. https://doi.org/10.1155/2015/647958
38. Bruehlmeier M, Dietz V, Leenders KL, Roelcke U, Missimer J, Curt A (1998) How does the human brain deal with a spinal cord injury? Eur J Neurosci 10:3918–3922. https://doi.org/10.1046/j.1460-9568.1998.00454.x
39. Cramer SC, Lastra L, Lacourse MG, Cohen MJ (2005) Brain motor system function after chronic, complete spinal cord injury. Brain 128:2941–2950. https://doi.org/10.1093/brain/awh648
40. Bunday KL, Tazoe T, Rothwell JC, Perez MA (2014) Subcortical control of precision grip after human spinal cord injury. J Neurosci 34:7341–7350. https://doi.org/10.1523/JNEUROSCI.0390-14.2014
41. Dobkin BH (2000) Spinal and supraspinal plasticity after incomplete spinal cord injury: correlations between functional magnetic resonance imaging and engaged locomotor networks. Prog Brain Res 128:99–111. https://doi.org/10.1016/S0079-6123(00)28010-2
42. Curt A, Alkadhi H, Crelier GR, Boendermaker SH, Hepp-Reymond MC, Kollias SS (2002) Changes of non-affected upper limb cortical representation in paraplegic patients as assessed by fMRI. Brain 125:2567–2578. https://doi.org/10.1093/brain/awf250
43. Holly LT, Dong Y, Albistegui-DuBois R, Marehbian J, Dobkin B (2014) Cortical reorganization in patients with cervical spondylotic myelopathy. J Neurosurg Spine 6:544–551. https://doi.org/10.3171/spi.2007.6.6.5.Cortical
44. Henderson LA, Gustin SM, Macey PM, Wrigley PJ, Siddall PJ (2011) Functional reorganization of the brain in humans following spinal cord injury: evidence for underlying changes in cortical anatomy. J Neurosci 31:2630–2637. https://doi.org/10.1523/JNEUROSCI.2717-10.2011
45. Wurster CD, Graf H, Ackermann H, Groth K, Kassubek J, Riecker A (2015) Neural correlates of rate-dependent finger-tapping in Parkinson's disease. Brain Struct Funct 220:1637–1648. https://doi.org/10.1007/s00429-014-0749-1
46. Nikolaidis I, Fouyas IP, Sandercock PA, Statham PF (2010) Surgery for cervical radiculopathy or myelopathy. Cochrane Database Syst Rev CD001466. https://doi.org/10.1002/14651858.CD001466.pub3
47. Dhillon RS, Parker J, Syed YA et al (2016) Axonal plasticity underpins the functional recovery following surgical decompression in a rat model of cervical spondylotic myelopathy. Acta Neuropathol Commun 4:89. https://doi.org/10.1186/s40478-016-0359-7
48. Martin AR, Aleksanderek I, Cohen-Adad J et al (2016) Translating state-of-the-art spinal cord MRI techniques to clinical use: a systematic review of clinical studies utilizing DTI, MT, MWF, MRS, and fMRI. Neuroimage Clin 10:192–238. https://doi.org/10.1016/j.nicl.2015.11.019